

## Assembly Pattern of Supramolecular Hydrogel Induced by Lower Critical Solution Temperature Behavior of Low-Molecular-Weight Gelator

Shuanggen Wu, Qiao Zhang, Yan Deng, Xing Li, Zheng Luo, Bo Zheng, and Shengyi Dong

*J. Am. Chem. Soc.*, **Just Accepted Manuscript** • DOI: 10.1021/jacs.9b11290 • Publication Date (Web): 11 Dec 2019

Downloaded from [pubs.acs.org](https://pubs.acs.org) on December 11, 2019

### Just Accepted

“Just Accepted” manuscripts have been peer-reviewed and accepted for publication. They are posted online prior to technical editing, formatting for publication and author proofing. The American Chemical Society provides “Just Accepted” as a service to the research community to expedite the dissemination of scientific material as soon as possible after acceptance. “Just Accepted” manuscripts appear in full in PDF format accompanied by an HTML abstract. “Just Accepted” manuscripts have been fully peer reviewed, but should not be considered the official version of record. They are citable by the Digital Object Identifier (DOI®). “Just Accepted” is an optional service offered to authors. Therefore, the “Just Accepted” Web site may not include all articles that will be published in the journal. After a manuscript is technically edited and formatted, it will be removed from the “Just Accepted” Web site and published as an ASAP article. Note that technical editing may introduce minor changes to the manuscript text and/or graphics which could affect content, and all legal disclaimers and ethical guidelines that apply to the journal pertain. ACS cannot be held responsible for errors or consequences arising from the use of information contained in these “Just Accepted” manuscripts.

# Assembly Pattern of Supramolecular Hydrogel Induced by Lower Critical Solution Temperature Behavior of Low-Molecular-Weight Gelator

Shuanggen Wu,<sup>a</sup> Qiao Zhang,<sup>a</sup> Yan Deng,<sup>a</sup> Xing Li,<sup>a</sup> Zheng Luo,<sup>a</sup> Bo Zheng,<sup>b\*</sup> and Shengyi Dong<sup>a\*</sup>

<sup>a</sup>College of Chemistry and Chemical Engineering, Hunan University, Changsha, Hunan 410082, P. R. China

<sup>b</sup>Key Laboratory of Synthetic and Natural Functional Molecule Chemistry of the Ministry of Education, College of Chemistry and Materials Science, Northwest University, Xi'an 710069, P. R. China.

*Supporting Information Placeholder*

**ABSTRACT:** Although the gelation process and lower critical solution temperature (LCST) behavior are well acknowledged in polymer systems, low-molecular-weight gelators (LMWGs) rarely display LCST behavior during supramolecular gelation. Herein, we report an LMWG system with LCST-type thermo-responsiveness and an LCST-triggered supramolecular gelation process. Temperature plays a crucial role in this system, not only affecting the LCST phase separation, but also triggering the gelation process. The backbones (three-dimensional structures) of the resulting hydrogel are the hierarchical assemblies of the LMWG undergoing the LCST phase separation. Hence, the gelation of the LMWG is only realized when the gelation temperature is above the critical transition temperature ( $T_{\text{cloud}}$ ) of the LCST behavior, which is different to many supramolecular or polymeric hydrogel systems.

## INTRODUCTION

Hydrogels are found ubiquitously in biological systems as multifunctional materials.<sup>1-3</sup> Many artificial gelators and gelation strategies have been applied in recent decades to fabricate supramolecular hydrogel materials.<sup>4-9</sup> The reversible gel-sol transitions triggered by external stimuli are key steps to realize controlled self-assembly and functionalization.<sup>10-15</sup> The thermo-responsive property of hydrogel structures is frequently introduced to artificial hydrogel systems to perform gel-sol transitions that are used for drug release, self-healing, shape memory, and supramolecular adhesion.<sup>16-20</sup>

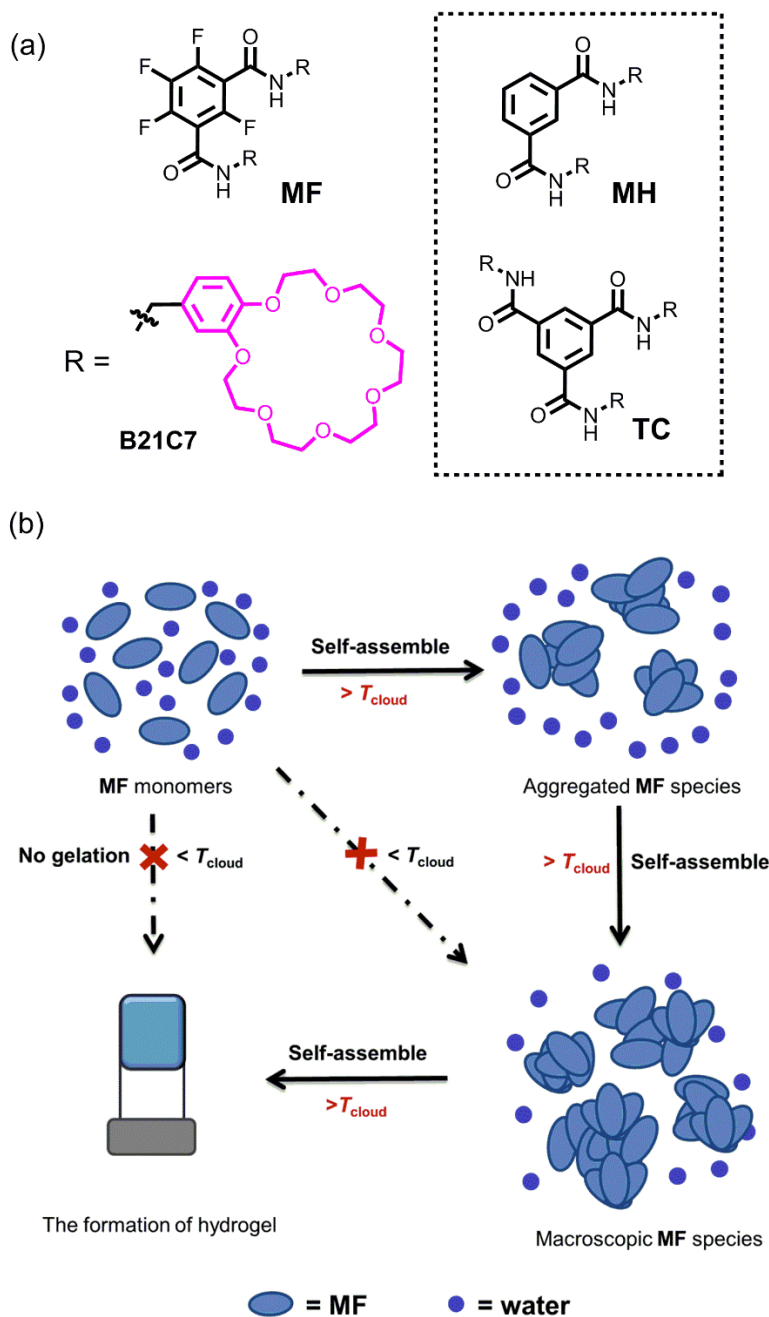
Compared with the common gel-sol transitions simply triggered by heating/cooling, the combination of gelation behavior and lower critical solution temperature (LCST)-type thermo-responsiveness endows hydrogels with a unique property of thermo-responsiveness: thermo-responsiveness is achieved and maintained without gel-sol transitions.<sup>21-25</sup> For example, Wang *et al.* reported poly(*N*-isopropylacrylamide) (PNIPAm)-based supramolecular gels with LCST-type properties, which are available for smart windows.<sup>25</sup> Such heating/cooling-induced transparent-turbid transitions of supramolecular gels need a sophisticated molecular design because supramolecular hydrogels are sensitive to elevated temperature and would be destroyed at high temperature.<sup>26-32</sup> Until now, LCST-type supramolecular gels are mainly restricted to PNIPAm family, because PNIPAm and its derivatives have a critical transition temperature ( $T_{\text{cloud}}$ ) of approximately 30–37 °C.<sup>33-36</sup> In this temperature range, supramolecular hydrogels easily maintain the gel morphol-

ogy.<sup>37-39</sup> However, in polymeric hydrogel systems with LCST behaviors, the gelation process and LCST behavior are usually two independent phenomena and do not interfere with each other. In other words, the formation of hydrogels is not triggered by the LCST behavior and the critical gelation temperature is always below the  $T_{\text{cloud}}$  of LCST behavior. Low-molecular weight-gelators (LMWGs) are less explored to fabricate LCST-type supramolecular hydrogels, though they may provide more opportunities for the design of advanced functional systems with desired structures and functions.<sup>40-42</sup> The restrictions for the exploration of LCST-type supramolecular hydrogels based on LMWGs are: a) it is difficult to design a small molecule that possesses gelation and LCST capacities simultaneously and b) the gelation processes of LMWGs are rich with ambiguity when LCST behavior coexists.

In general, to display LCST behavior in water, (macro)molecules are required to form hydrogen bonds with water molecules, whereas strong water-participant hydrogen bonding is unfavorable for the supramolecular gelation.<sup>43,44</sup> During the gelation process, gelators aggregate together *via* intermolecular interactions to form three-dimensional structures (typical processes of supramolecular gels; such structures can further assemble to macroscopic gel materials);<sup>45</sup> however, strong gelator-water hydrogen bonding (hydration effect) can weaken or destroy the intermolecular aggregation.<sup>46</sup> Considering the above-mentioned facts, the molecular design is required to handle the conflict and elegantly balance the two competing parts. Amphiphilic structures may be ideal candidates to overcome these problems because their hydrophilic peripheral parts can interact with water molecules to realize LCST behavior, and the hydrophobic core of the gelator remains insulated from water molecules and assembles to form the gel without the interruption by water molecules. With suitable thermo-responsive segments, the fabrication of LMWGs-based LCST-type supramolecular hydrogels is possible.

Herein, we report an LMWG system with LCST-type thermo-responsiveness and an unexpected LCST-induced supramolecular gelation process. Firstly, the critical transition temperature ( $T_{\text{cloud}}$ ) of the LMWG can be easily modulated, and the hydrogel maintains its gel morphology over the temperature range being tested. Therefore, the LCST-type phase behaviors of this system are observed in both sol and gel states. Secondly, the gelation process of the LMWG is realized only when the gelation temperature is above  $T_{\text{cloud}}$ . The LCST behavior of the LMWG results in the formation of visible macroscopic aggregates in sol state, whereas in the subsequent gelation process, these macroscopic aggregates of LMWG

1 molecules transform into the three-dimensional structures of hydro-  
 2 gel. Once the gelation temperature is below  $T_{\text{cloud}}$  due to the disap-  
 3 pearance of macroscopic aggregates, no supramolecular hydrogels  
 4 are formed. This LMWG system is different to previously reported  
 5 polymeric hydrogels with LCST,<sup>21-25</sup> as in this system LCST be-  
 6 havior is closely related to the formation of supramolecular hydro-  
 7 gels.



**Scheme 1.** (a) Chemical structures of LMWG MF and model compounds (TC and MH) and (b) LCST-induced supramolecular gelation: gelation of MF is only realized when the gelation temperature is above the critical transition temperature ( $T_{\text{cloud}}$ ) of LCST behavior.

## RESULTS AND DISCUSSION

**Monomer design.** Benzo-21-crown-7 (B21C7) derivatives are a new class of LCST molecules and are used in different systems to facilitate LCST behavior.<sup>46</sup> Amphiphilic monomers with two B21C7 units are designed and synthesized via amidation reactions from the corresponding benzenedicarboxylic acid (MF in Scheme 1a). Hydrophilic B21C7 units, located on the outer layer, are used as the thermo-responsive segments to display LCST phase behavior,

while the hydrophobic tetrafluorobenzene with amide linkers, located in the inner layer, controls the aggregation of gelators to realize supramolecular gelation through F–F interactions,  $\pi$ – $\pi$  stacking, and hydrophobic interactions. MF achieves a balance between the solubility (hydration effect) and aggregation (gelation process), according to the solubility test and gelation performances, which is suitable for the investigation of LCST-triggered supramolecular gelation.<sup>47</sup>

**LCST behavior of MF in sol and gel states.** The preliminary results are observed by heating/cooling MF aqueous solutions directly. The water solution of MF displays LCST phase separation when the temperature was elevated/decreased, with reversible transparent-turbid transitions as typical phenomena (Figure 1a, left).<sup>46</sup> In detail, the transmittance data of MF solutions, shown in Figures 1b,c, recorded using a UV/Vis spectrometer confirm such LCST behavior, with a dramatic decrease in transmittance above  $T_{\text{cloud}}$ . The concentration-dependent UV/Vis measurements (Figure 1b, S12) demonstrate a wide distribution of  $T_{\text{cloud}}$  from less than 20 °C to more than 50 °C (concentration of MF varies from 8.0 to 2.0 mg/mL). MF at 8.0 mg/mL has a  $T_{\text{cloud}}$  of 18.9 °C upon heating or 16.2 °C upon cooling (Figure 1c). Further increase in the concentration of MF shows only a slight influence on  $T_{\text{cloud}}$  and transition windows ( $T_{\text{cloud}}$  of MF at 12 mg/mL is 18.7 °C). The structural integrity and aggregation reversibility of MF are confirmed by repeated heating-cooling cycles (Table S1).

Interestingly, the turbid MF solution gradually turns into a turbid gel, as confirmed by the tube inversion test, scanning electron microscopic (SEM), transmission electron microscopic (TEM) and rheological measurements (Figure 1a, middle, Figure S13, S14 and S15).<sup>45,48</sup> Three dimensional networks of fibers were observed (Figure S13 and S14). The gelation process of MF at 25 °C is slow (8.0 mg/mL, 9 h). Meanwhile, the turbidity of the sample exists during the whole gelation process, indicating the concomitant occurrence of the LCST behavior. However, no gelation behavior was observed at 4 °C, 10 °C, or 15 °C (8.0 mg/mL, a transparent MF solution, tested for 72 h), which is in contrast to the common supramolecular gelation processes.<sup>40-42</sup> The MF solutions with different concentrations (6.0 mg/mL and 12 mg/mL, 10 h and 8 h, respectively) only become hydrogel gels (turbid) when temperatures are above  $T_{\text{cloud}}$ .

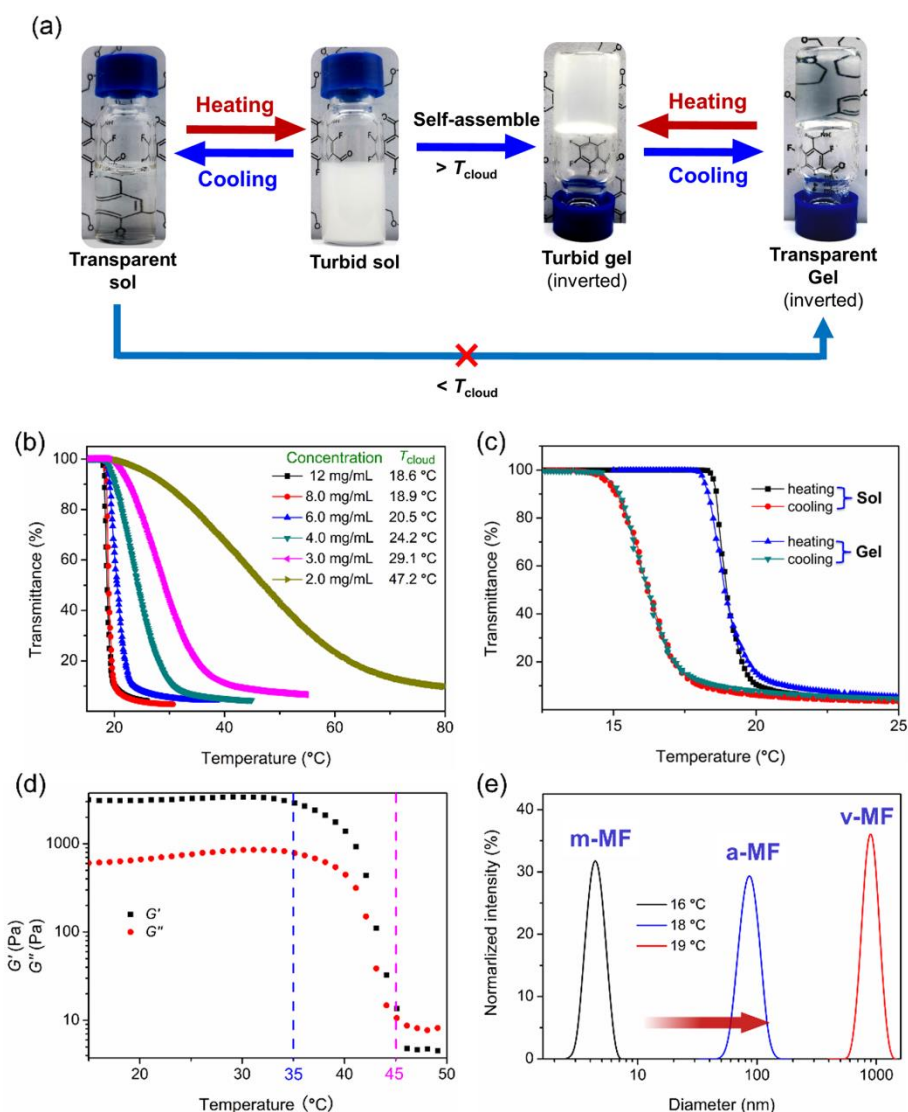


**Figure 1.** LCST and gelation behavior of MF: (a) macroscopic LCST-induced gelation of MF sol and gel; (b) concentration-dependent turbidity curves of MF with heating rate of 1.0 °C/min; (c) heating-cooling cycles of MF (8.0 mg/mL) at sol and gel states, with heating/cooling rate of 1.0 °C/min; (d) temperature-dependent rheology tests of MF gel (8.0 mg/mL); (e) temperature-dependent DLS of MF at a concentration of 8.0 mg/mL. Here m-MF, a-MF, and v-MF represent the monomer-type MF, aggregated MF, and visible MF, respectively.

The MF hydrogel of concentration 8.0 mg/mL (prepared at 25 °C) displays a typical LCST-type behavior after cooling (Figure 1a, right): the opaque hydrogel gradually turns translucent, and finally

becomes transparent. The entire turbid-transparent transition of the MF hydrogel is completely reversible. Rheological characterization of MF further provides quantitative information on the storage

moduli ( $G'$ ) and loss moduli ( $G''$ ):  $G'$  values are higher than  $G''$  values over the entire experimental range of frequencies and independent of frequencies (Figure S13). As shown in Figure 1c, the  $T_{\text{cloud}}$  of the MF hydrogel is close to that of the MF solution at the same concentration (8.0 mg/mL). The turbidity curves of the MF solution and MF hydrogel at different heating rates (ranging from 0.1 to 2.0 °C/min, 8.0 mg/mL for MF) are very similar, too. During the heating process (15 to 35 °C), the hydrogel retains its bulky morphology, and no gel–sol transitions or collapsed gels are observed (Figure 1a, right). The rheological tests of MF hydrogels at variable temperature confirm the stability of hydrogels during the heating process until the temperature exceeds 35 °C (Figure 1d). Such heating-induced transition from gel to sol is concentration-dependent. When the concentration of MF was increased from 8.0 mg/mL to 24 mg/mL, the hydrogel is more stable to the elevated temperature. Macroscopic tests are consistent with the rheological tests: when the temperature was increased from 15 to 35 °C, the hydrogel still kept its bulky morphology (8.0 mg/mL), and only the light transmittance of the hydrogel gradually decreased.

**LCST-type supramolecular gelation process.** The aggregation processes at different states were easily followed and monitored because of the slow gelation process of MF at 8.0 mg/mL (25 °C, 9 h). First, the investigations of MF in the sol state were carried out. Particles with an average size of 3–4 nm in MF solution at temperature below 16 °C were clearly noted from the dynamical lighting scattering (DLS) result (Figure 1e), indicating that MF molecules exist as monomer types without any aggregation. When the temperature was changed to 18 °C, large aggregates with an average size of approximately 80 nm were recorded. The tyndall effect was observed at this temperature, whereas no obvious turbidity was visible to the naked eye. However, when the temperature was increased to 19 °C, slightly above  $T_{\text{cloud}}$ , not only were micrometer-sized particles detected, but the macroscopic transition from a transparent solution to a turbid mixture was also observed.

According to the DLS data, it is obvious that an aggregation process was induced during heating in the sol state, accompanied with the size enhancement from invisible monomer-type MF (m-

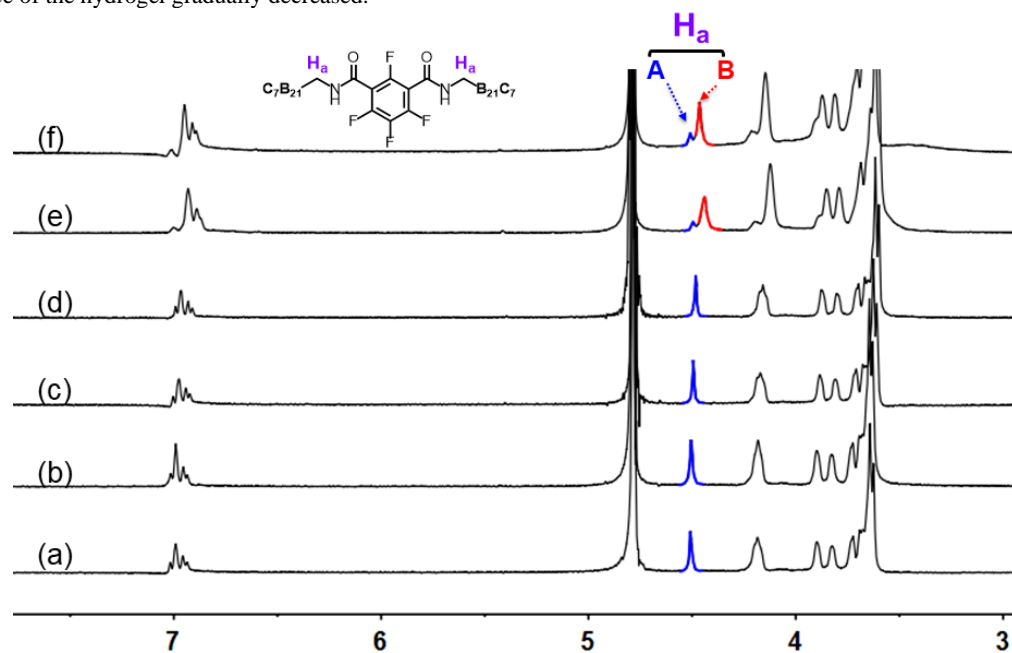


**Figure 2.** Concentration-dependent  $^1\text{H}$  NMR spectra ( $\text{D}_2\text{O}$ , 400 MHz, 25 °C) of MF: (a) 1.4 mg/mL, (b) 3.0 mg/mL, (c) 4.0 mg/mL, (d) 5.0 mg/mL, (e) 6.0 mg/mL, and (f) 8.0 mg/mL. Here peaks A and B are in blue and red, respectively.

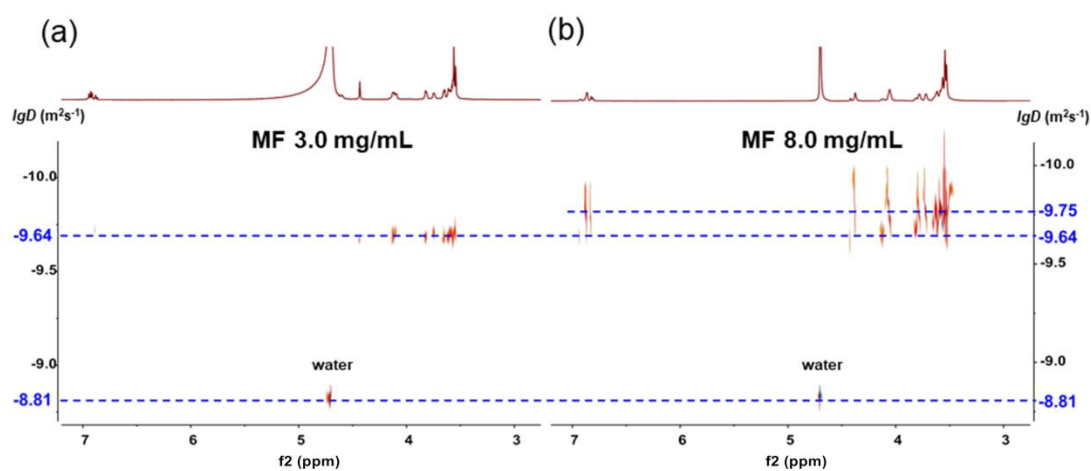


**Figure 3.** DOSY spectra ( $\text{D}_2\text{O}$ , 400 MHz, 25 °C) of MF: (a) 3.0 mg/mL, (b) 8.0 mg/mL. The same diffusion coefficients are obtained for residual water molecules.

**MF**, < 3–4 nm, Figure S17) to aggregated **MF** species (**a-MF**, < 80 nm), and finally to visible particles (**v-MF**, > 1  $\mu\text{m}$ ).

The nuclear magnetic resonance (NMR) experiments of freshly prepared samples were performed to get further insights into the gelation process. The concentration of the LMWG is an important factor that affects the gelation process and the property of the supramolecular gel. During the concentration-dependent NMR tests, all **MF** samples were in the sol state. When the concentrations of **MF** samples were between 1.4 mg/mL and 5.0 mg/mL, no remarkable changes in NMR spectra were observed because no apparent chemical shifts or new peaks emerged (Figure 2, S16). Different NMR spectra were obtained when the concentrations of **MF** samples were further increased. With protons  $H_a$  ( $-\text{CONH}_2\text{CH}_2-$ ) as an example (Figure 2), the former single peak of  $H_a$  split into two sets (peaks A and B) when the **MF** concentration varied to 6.0 mg/mL and 8.0 mg/mL.

The diffusion ordered spectroscopy (DOSY) experiments of **MF** (3.0 mg/mL and 8.0 mg/mL) were carried out at 25  $^\circ\text{C}$  (Figure 3).

The diffusion coefficient ( $D$ ) of **MF** at 3.0 mg/mL is  $2.29 \times 10^{-10} \text{ m}^2/\text{s}$ , corresponding to the size of 1.82 nm.<sup>46</sup> Two sets of  $D$  were obtained from the **MF** spectra at 8.0 mg/mL:  $2.29 \times 10^{-10} \text{ m}^2/\text{s}$  (1.82 nm, peak A) and  $1.78 \times 10^{-10} \text{ m}^2/\text{s}$  (2.24 nm, peak B). The simulation results demonstrate that the size of a single **MF** molecule is smaller than 2.5 nm (Figure S17). The DOSY results indicate that both peaks A and B belong to the monomer-type **MF** (**m-MF**).  $^1\text{H}$  NMR spectrum of **MF** at 15  $^\circ\text{C}$  (<  $T_{\text{cloud}}$  of **MF** at 8.0 mg/mL) also shows peaks A and B, indicating that the occurrence of peak B is not the result of LCST phase behavior. Hence, these changes of concentration-dependent NMR spectra can be ascribed to a concentration-induced molecular transformation of **MF**.

During the concentration-dependent and DOSY NMR tests, all **MF** samples were in sol state. The time-/temperature-dependent NMR tests of **MF** were carried out to monitor the LCST-induced supramolecular gelation (Figure 4, S18–24), respectively. With residual water as the standard in the time-dependent NMR spectra, the normalized intensity of **MF** was plotted. As shown in Figure

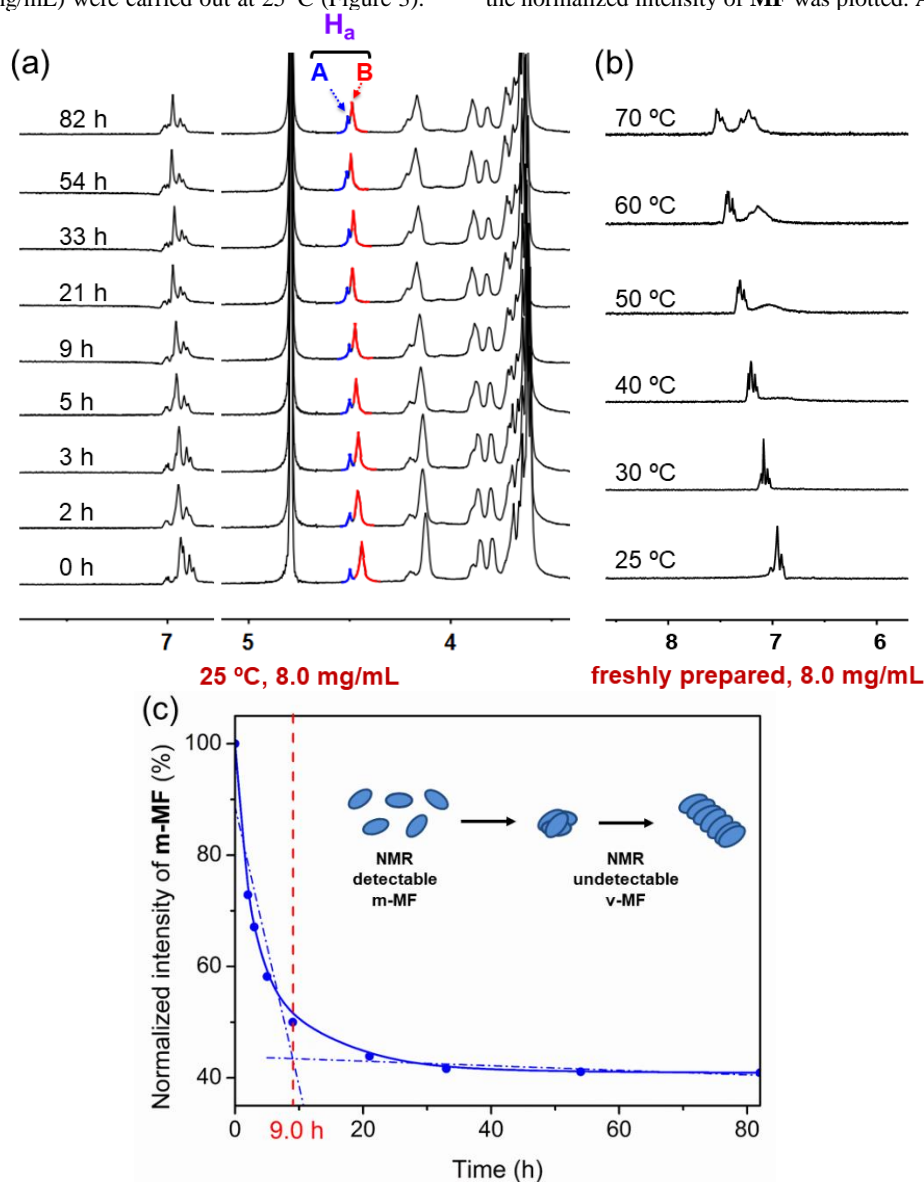


**Figure 4.** (a) Partial time-dependent  $^1\text{H}$  NMR spectra ( $\text{D}_2\text{O}$ , 400 MHz, 25  $^\circ\text{C}$ ) of **MF**; (b) Partial temperature-dependent  $^1\text{H}$  NMR spectra ( $\text{D}_2\text{O}$ , 400 MHz) of **MF**. The concentrations of **MF** for (a) and (b) are 8.0 mg/mL. Here peaks A and B (**m-MF**) are in blue and red, respectively. (c) Normalized intensity of **m-MF** (peaks A and B in Figure 4a).

4c, the intensity of **m-MF** (the total intensities of peaks A and B) rapidly decreases during first 9 h, then gradually reaches equilibrium. This observation indicates that more and more **MF** molecules are not detected during the time-dependent NMR tests.

Two possibilities are envisioned to explain the disappearance of **MF** molecules in the NMR spectra:

(A) In our previous work, we have found that micrometer-sized aggregates are NMR undetectable and phase-separated from the LCST solution when temperature is above  $T_{\text{cloud}}$ .<sup>46</sup> Based on the DLS results and our previous work, the appearance of NMR undetectable **MF** molecules may be ascribed to the formation of micrometer-sized aggregates (**v-MF**, detected by DLS,  $> 1 \mu\text{m}$ ) that were phase separated from the **MF** NMR samples.

(B) During the time-dependent NMR tests, the NMR sample solution (8.0 mg/mL) gradually changed into a mixture of gel and sol, then completely into gel state. The **MF** molecules may assemble into the three-dimensional structures of hydrogels (solid parts of hydrogels) that are also NMR undetectable as proved by some reported work.<sup>45,49,50</sup>

**TC** and **MH** are analogues of **MF** and are used as control compounds to evaluate the possibilities for the disappearance of **MF** molecules in NMR spectra (Scheme 1 and Figure S25–27).<sup>46</sup> **TC** and **MH** display LCST behavior; however, they cannot form hydrogels at either low temperature or above  $T_{\text{cloud}}$ . Both **TC** and **MH** show decreased intensities of NMR signals when the temperature is above  $T_{\text{cloud}}$  as monitored by NMR (Figure S27).<sup>46</sup> Without the disturbance of the formation of three-dimensional structures of hydrogels, the disappearance of **TC** or **MH** molecules in NMR spectra is ascribed to the formation of micrometer-sized aggregates (phase-separated from the LCST solution upon heating).<sup>46</sup> Considering the large aggregates of **v-MF** observed in DLS tests and the phase-separation of **MF** sample during time-dependent NMR tests, it can be speculated that large **v-MF** aggregates are responsible for the disappearance of **MF** molecules in NMR spectra when the temperature was above  $T_{\text{cloud}}$  (Possibility A, induced by LCST behavior).

However, this explanation only describes half of the picture. Different NMR changes were observed in the temperature-dependent NMR spectra of **MF** (in sol state without any gelation behavior, Figure 4b, S21–24) compared to that of the time-dependent NMR spectra (with gelation behavior). As temperature gradually increased from 40 °C to 70 °C, new proton peaks appear in the temperature-dependent NMR spectra of **MF**, as shown in Figure 4b. As mentioned above, the **MF** hydrogels are stable below 35 °C (Figure 1e, 8.0 mg/mL), hence during this temperature range, no gel formation was possible. These newly emerging peaks were also found in the temperature-dependent NMR spectra of **MH** and **TC** (Figure S27). However, no changes were observed from the time-dependent NMR spectra of **MH** or **TC** (Figure S25, 25 °C), which is different to **MF** (Figure 4a).<sup>46</sup> This information indicates that without gel formation (above 40 °C), **MF** behaves the same as pure LCST systems like **MH** or **TC**. While once gel formation occurred (25 °C), LCST behavior of **MF** is not the same as that of **MH** or **TC**.<sup>46</sup>

As mentioned above, during the gelation tests, we have found that the NMR sample solution (8.0 mg/mL) failed to form hydrogel when the temperature was set at 15 °C, 10 °C, or 4 °C (no LCST behavior). In additional, **MF** solutions with lower concentrations (1.0 mg/mL or 3.0 mg/mL, Figures S18 and S19) showed neither apparent changes during time-dependent NMR tests nor become hydrogels. These observations indicated that once **v-MF** species were absent due to the lower temperature or concentration, **MF** could not assemble into three-dimensional structures of hydrogels. Such observations are quite different to PNIPAm hydrogels. In these polymeric systems, the formation of hydrogels is dependent

on the structures of PNIPAm (cross-linked polymers). LCST behavior of PNIPAm usually takes place after the formation of hydrogels.<sup>25,26</sup>

Generally, hydrogels consist of two parts: solid-type three-dimensional structures (backbones of hydrogels, NMR undetectable) and solution-type entrapped solvents and LMWGs (sol parts of hydrogels, NMR detectable). In the sol part of the hydrogel of **MF**, the concentration of entrapped **MF** molecules is only 4.0 mg/mL (Figure S28), which is only half of the initial concentration of **MF** (8.0 mg/mL of **MF** when preparing the hydrogel sample), indicating that the concentration of **MF** in three-dimensional structures is much higher than that in the sol part. Based on these information, it is highly possible that **v-MF** species induced by LCST behavior can further self-assemble into the solid-parts (NMR undetectable three-dimensional structures) of hydrogels (Possibility B, induced by the gelation process), and the rest of **MF** molecules are entrapped in the sol-parts (NMR detectable).<sup>45,47</sup>

As mentioned before, two types of **MF** species are identified: **m-MF** (peaks A and B, NMR detectable) and **v-MF** (visible but NMR undetectable). Corresponding peaks in DLS of these species are of sizes below 3–4 nm (**m-MF**) and above 1  $\mu\text{m}$  (**v-MF**), respectively. In this LMWG system, temperature orchestrates a two-step hierarchical assembly, the LCST behavior and the gelation process. During the gelation process, the LCST behavior of **MF** is crucial in realizing the gelation process because the backbones of hydrogels are comprised of LCST-induced aggregation of **v-MF**. In this **MF** hydrogel system, these NMR undetectable **v-MF** aggregates become the turbid phase and the solid-type backbones of supramolecular hydrogels. **m-MF** molecules are entrapped in hydrogels as the sol part. Compared with some reported supramolecular polymer gels, **MF** hydrogels are non-viscous (because no polymerization process occurred) but with good mechanical strengths ( $G'$  up to  $3 \times 10^3$  Pa was observed). **MF** hydrogels at low temperature have a good light transmittance (Table S1).

## CONCLUSIONS

In conclusion, we report the LCST-induced supramolecular gelation process of a low-molecular-weight gelator **MF**. The reversible transparent-turbid transitions occurred in both sol and gel states. Different types of **MF** aggregates were observed during the LCST-induced gelation process. The LCST behavior of this hydrogel system plays a key role in the supramolecular gelation by forming macroscopic backbones of hydrogels, which is rarely observed in polymeric or supramolecular hydrogel systems. The macroscopic aggregates induced by the LCST phase separation behavior transform into the three-dimensional structures of hydrogels. This research not only proves the feasibility of LMWGs in realizing the LCST-type thermo-responsiveness besides acrylamide-containing thermo-responsive polymers, but also provides a clear view of the LCST-type gelation process. Furthermore, this new class of thermo-responsive LMWGs provides different insights into the gelation mechanism of supramolecular hydrogels and represents a new choice of the design of thermo-sensitive supramolecular system.

## ASSOCIATED CONTENT

### Supporting Information

The Supporting Information is available free of charge on the ACS Publications website.

Experimental procedures, characterization and NMR spectra for obtained compounds and other materials (PDF)

## AUTHOR INFORMATION

## Corresponding Author

\* dongsy@hnu.edu.cn  
\* zhengbo@nwu.edu.cn

## ORCID

Shengyi Dong: 0000-0002-8640-537X

## Notes

The authors declare no competing financial interests.

## ACKNOWLEDGMENT

This work was supported by National Natural Science Foundation of China (21704024), Huxiang Young Talent Program from Hunan Province (2018RS3036), the Fundamental Research Funds for the Central Universities from Hunan University, and the 1000 Talents Award of Shaan'xi Province (334041900005).

## REFERENCES

- (1) Bhattacharya, S.; Samanta, S. K. Soft-Nanocomposites of Nanoparticles and Nanocarbons with Supramolecular and Polymer Gels and Their Applications. *Chem. Rev.* **2016**, *116*, 11967–12028.
- (2) Hirst, A. R.; Escuder, B.; Miravet, J. F.; Smith, D. K. High-Tech Applications of Self-Assembling Supramolecular Nanostructured Gel-Phase Materials: From Regenerative Medicine to Electronic Devices. *Angew. Chem. Int. Ed.* **2008**, *47*, 8002–8018.
- (3) Ma, X.; Zhao, Y. Biomedical Applications of Supramolecular Systems Based on Host–Guest Interactions. *Chem. Rev.* **2015**, *115*, 7794–7839.
- (4) Döring, A.; Birnbaum, W.; Kuckling, D. Responsive Hydrogels-Structurally and Dimensionally Optimized Smart Frameworks for Applications in Catalysis, Micro-System Technology and Material Science. *Chem. Soc. Rev.* **2013**, *42*, 7391–7420.
- (5) Foster, J. A.; Parker, R. M.; Belenguer, A. M.; Kishi, N.; Sutton, S.; Abell, C.; Nitschke, J. R. Differentially Addressable Cavities within Metal-Organic Cage-Cross-Linked Polymeric Hydrogels. *J. Am. Chem. Soc.* **2015**, *137*, 9722–9729.
- (6) Zhou, J.; Du, X.; Gao, Y.; Shi, J.; Xu, B. Aromatic-Aromatic Interactions Enhance Interfiber Contacts for Enzymatic Formation of a Spontaneously Aligned Supramolecular Hydrogel. *J. Am. Chem. Soc.* **2014**, *136*, 2970–2973.
- (7) Xu, W.; Song, Q.; Xu, J.-F.; Serpe, M. J.; Zhang, X. Supramolecular Hydrogels Fabricated from Supramonomers: A Novel Wound Dressing Material. *ACS Appl. Mater. Interfaces* **2017**, *9*, 11368–11372.
- (8) Sun, J.-Y.; Zhao, X.; Illeperuma, W. R. K.; Chaudhuri, O.; Oh, K. H.; Mooney, D. J.; Vlassak, J. J.; Suo, Z. Highly Stretchable and Tough Hydrogels. *Nature* **2012**, *489*, 133–136.
- (9) Ke, H.; Yang, L.-P.; Xie, M.; Chen, Z.; Yao, H.; Jiang, W. Shear-Induced Assembly of a Transient yet Highly Stretchable Hydrogel Based on Pseudopolyrotaxanes. *Nat. Chem.* **2019**, *11*, 470–477.
- (10) Coates, I. A.; Smith, D. K. Controlled Self-Assembly-Synthetic Tunability and Covalent Capture of Nanoscale Gel Morphologies. *Chem. Eur. J.* **2009**, *15*, 6340–6344.
- (11) Zhang, Q.; Qu, D.-H.; Wu, J.; Ma, X.; Wang, Q.; Tian, H. A Dual-Modality Photoswitchable Supramolecular Polymer. *Langmuir* **2013**, *29*, 5345–5350.
- (12) Du, X.; Zhou, J.; Shi, J.; Xu, B. Supramolecular Hydrogelators and Hydrogels: From Soft Matter to Molecular Biomaterials. *Chem. Rev.* **2015**, *115*, 13165–13307.
- (13) Matsumoto, K.; Sakikawa, N.; Miyata, T. Thermo-Responsive Gels That Absorb Moisture and Ooze Water. *Nat. Commun.* **2018**, *9*, 2315.
- (14) Komatsu, H.; Matsumoto, S.; Tamaru, S.; Kaneko, K.; Ikeda, M.; Hamachi, I. Supramolecular Hydrogel Exhibiting Four Basic Logic Gate Functions To Fine-Tune Substance Release. *J. Am. Chem. Soc.* **2009**, *131*, 5580–5585.
- (15) Yan, X.; Xu, D.; Chi, X.; Chen, J.; Dong, S.; Ding, X.; Yu, Y.; Huang, F. A Multiresponsive, Shape-Persistent, and Elastic Supramolecular Polymer Network Gel Constructed by Orthogonal Self-Assembly. *Adv. Mater.* **2012**, *24*, 362–369.
- (16) Draper, E. R.; Adams, D. J. How Should Multicomponent Supramolecular Gels Be Characterised? *Chem. Soc. Rev.* **2018**, *47*, 3395–3405.
- (17) Montero de Espinosa, L.; Meesom, W.; Moatsou, D.; Weder, C. Bio-inspired Polymer Systems with Stimuli-Responsive Mechanical Properties. *Chem. Rev.* **2017**, *117*, 12851–12892.

- (18) Lu, C.-H.; Guo, W.; Hu, Y.; Qi, X.-J.; Willner, I. Multitriggered Shape-Memory Acrylamide-DNA Hydrogels. *J. Am. Chem. Soc.* **2015**, *137*, 15723–15731.
- (19) Jia, Y.-G.; Zhu, X. Self-Healing Supramolecular Hydrogel Made of Polymers Bearing Cholic Acid and  $\beta$ -Cyclodextrin Pendants. *Chem. Mater.* **2015**, *27*, 387–393.
- (20) Zhang, M.; Xu, D.; Yan, X.; Chen, J.; Dong, S.; Zheng, B.; Huang, F. Self-Healing Supramolecular Gels Formed by Crown Ether Based Host–Guest Interactions. *Angew. Chem. Int. Ed.* **2012**, *51*, 7011–7015.
- (21) Fernández-Castaño Romera, M.; Göstl, R.; Shaikh, H.; ter Huurne, G.; Schill, J.; Voets, I. K.; Storm, C.; Sijbesma, R. P. Mimicking Active Biopolymer Structures with a Synthetic Hydrogel. *J. Am. Chem. Soc.* **2019**, *141*, 1989–1997.
- (22) Karimi, M.; Zangabad, P. S.; Ghasemi, A.; Amiri, M.; Bahrami, M.; Malekzad, H.; Asl, H. G.; Mahdiz, Z.; Bozorgomid, M.; Ghasemi, A.; Boyuk, M. R. T.; Hamblin, M. R. Temperature-Responsive Smart Nanocarriers for Delivery Of Therapeutic Agents: Applications and Recent Advances. *ACS Appl. Mater. Interfaces* **2016**, *8*, 21107–21133.
- (23) Hapiot, F.; Menuel, S.; Monflier, E. Thermoresponsive Hydrogels in Catalysis. *ACS Catal.* **2013**, *3*, 1006–1010.
- (24) Kitazawa, Y.; Ueki, T.; McIntosh, L. D.; Tamura, S.; Niitsuma, K.; Imaizumi, S.; Lodge, T. P.; Watanabe, M. Hierarchical Sol–Gel Transition Induced by Thermosensitive Self-Assembly of An ABC Triblock Polymer in an Ionic Liquid. *Macromolecules* **2016**, *49*, 1414–1423.
- (25) Wang, S.; Xu, Z.; Wang, T.; Xiao, T.; Hu, X.-Y.; Shen, Y.-Z.; Wang, L. Warm/Cool-Tone Switchable Thermochromic Material for Smart Windows by Orthogonally Integrating Properties of Pillar[6]Arene and Ferrocene. *Nat. Commun.* **2018**, *9*, 1737.
- (26) Zhang, Z.-X.; Liu, K. L.; Li, J. A Thermoresponsive Hydrogel Formed from a Star–Star Supramolecular Architecture. *Angew. Chem. Int. Ed.* **2013**, *52*, 6180–6184.
- (27) Du, P.; Liu, J.; Chen, G.; Jiang, M. Dual Responsive Supramolecular Hydrogel with Electrochemical Activity. *Langmuir* **2011**, *27*, 9602–9608.
- (28) Lorusson, T.; Jaksch, S.; Lübtow, M. M.; Jüngst, T.; Groll, J.; Lühmann, T.; Luxenhofer, R. A Thermogelling Supramolecular Hydrogel with Sponge-Like Morphology as a Cytocompatible Bioink. *Biomacromolecules* **2017**, *18*, 2161–2171.
- (29) Görl, D.; Soberats, B.; Herbst, S.; Stepanenko, V.; Würthner, F. Perylene Bisimide Hydrogels and Lyotropic Liquid Crystals with Temperature-Responsive Color Change. *Chem. Sci.* **2016**, *7*, 6786–6790.
- (30) Appel, E. A.; Biedermann, F.; Rauwald, U.; Jones, S. T.; Zayed, J. M.; Scherman, O. A. Supramolecular Cross-Linked Structures via Host–Guest Complexation with Cucurbit[8]Uril. *J. Am. Chem. Soc.* **2010**, *132*, 14251–14260.
- (31) Kiyonaka, S.; Sugiyasu, K.; Shinkai, S.; Hamachi, I. First Thermally Responsive Supramolecular Polymer Based on Glycosylated Amino Acid. *J. Am. Chem. Soc.* **2002**, *124*, 10954–10955.
- (32) Liu, J.; Chen, G.; Guo, M.; Jiang, M. Dual Stimuli-Responsive Supramolecular Hydrogel Based on Hybrid Inclusion Complex (HIC). *Macromolecules* **2010**, *43*, 8086–8093.
- (33) Zhang, X.-Z.; Xu, X.-D.; Cheng, S.-X.; Zhuo, R.-X. Strategies to Improve the Response Rate of Thermosensitive PNIPAAm Hydrogels. *Soft Matter* **2008**, *4*, 385–391.
- (34) Rosa, V. R.; Woisel, P.; Hoogenboom, R. Supramolecular Control over Thermoresponsive Polymers. *Mater. Today* **2016**, *19*, 44–55.
- (35) Noro, A.; Hayashi, M.; Matsushita, Y. Design and Properties of Supramolecular Polymer Gels. *Soft Matter* **2012**, *8*, 6416–6429.
- (36) Taylor, M. J.; Tomlins, P.; Sahota, T. S. Thermoresponsive Gels. *Gels* **2017**, *3*, 4.
- (37) Kawaguchi, H. Thermoresponsive Microhydrogels: Preparation, Properties and Applications. *Polym. Int.* **2014**, *63*, 925–932.
- (38) Haq, M. A.; Su, Y.; Wang, D. Mechanical Properties of PNIPAM based Hydrogels: A Review. *Mater. Sci. Eng. C* **2017**, *70*, 842–855.
- (39) Gandhi, A.; Paul, A.; Sen, S. O.; Sen, K. K. Studies on Thermoresponsive Polymers: Phase Behaviour, Drug Delivery and Biomedical Applications. *Asian J. Pharm. Sci.* **2015**, *10*, 99–107.
- (40) Draper, E. R.; Adams, D. J. Low-Molecular-Weight Gels: The State of the Art. *Chem.* **2017**, *3*, 390–410.
- (41) Estroff, L. A.; Hamilton, A. D. Water Gelation by Small Organic Molecules. *Chem. Rev.* **2004**, *104*, 1201–1218.
- (42) Piepenbrock, M.-O. M.; Lloyd, G. O.; Clarke, N.; Steed, J. W. Metal- and Anion-Binding Supramolecular Gels. *Chem. Rev.* **2010**, *110*, 1960–2004.
- (43) Shenoy, S. L.; Painter, P. C.; Coleman, M. M. The Swelling and Collapse of Hydrogen Bonded Polymer Gels. *Polymer* **1999**, *40*, 4853–4863.

(44) Krieg, E.; Bastings, M. M. C.; Besenius, P.; Rybtchinski, B. Supramolecular Polymers in Aqueous Media. *Chem. Rev.* **2016**, *116*, 2414–2477.

(45) Dong, S.; Luo, Y.; Yan, X.; Zheng, B.; Ding, X.; Yu, Y.; Ma, Z.; Zhao, Q.; Huang, F. A Dual-Responsive Supramolecular Polymer Gel Formed by Crown Ether Based Molecular Recognition. *Angew. Chem. Int. Ed.* **2011**, *50*, 1905–1909.

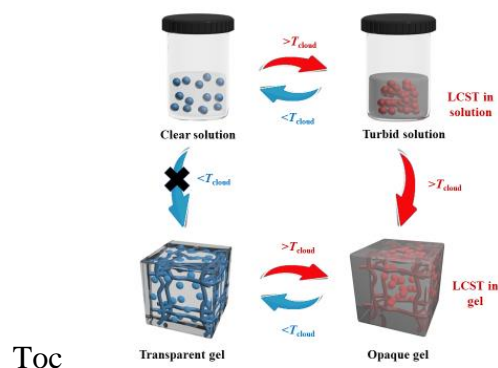
(46) Qi, Z.; Chiappisi, L.; Gong, H.; Pan, R.; Cui, N.; Ge, Y.; Bottcher, C.; Dong, S. Ion Selectivity in Nonpolymeric Thermosensitive Systems Induced by Water-Attenuated Supramolecular Recognition. *Chem. Eur. J.* **2018**, *24*, 3854–3861.

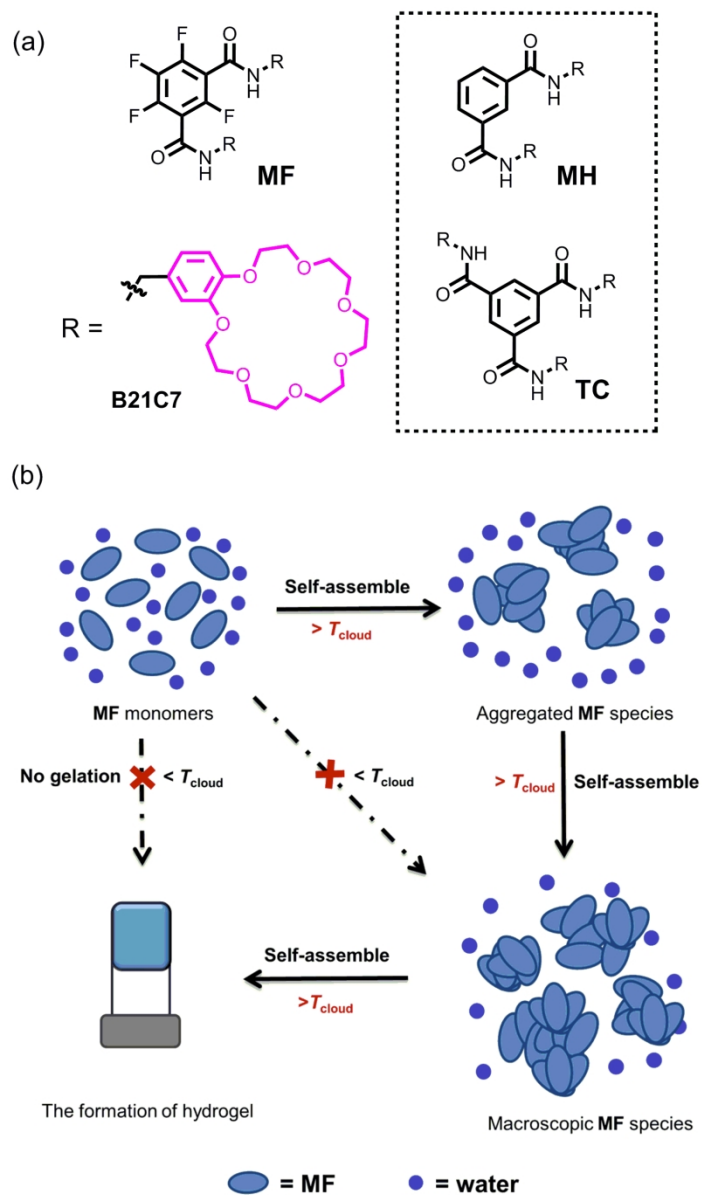
(47) Dong, S.; Leng, J.; Feng, Y.; Liu, M.; Stackhouse, C. J.; Schonhals, A.; Chiappisi, L.; Gao, L.; Chen, W.; Shang, J.; Jin, L.; Qi, Z.; Schalley, C. A. Structural Water as An Essential Comonomer in Supramolecular Polymerization. *Sci. Adv.* **2017**, *3*, eaao900.

(48) Yang, L.; Tan, X.; Wang, Z.; Zhang, X. Supramolecular Polymers: Historical Development, Preparation, Characterization, and Functions. *Chem. Rev.* **2015**, *155*, 7196–7239.

(49) Hirst, A. R.; Miravet, J. F. Escuder, B.; Noirez, L.; Castelletto, V.; Hamley, I. W.; Smith, D. K. Self-Assembly of Two-Component Gels: Stoichiometric Control and Component Selection. *Chem. Eur. J.* **2009**, *15*, 372–379.

(50) Raeburn, J.; Adams, D. J. Multicomponent Low Molecular Weight Gelators. *Chem. Commun.* **2015**, *51*, 5170–5180.





Scheme 1. (a) Chemical structures of LMWG MF and model compounds (TC and MH) and (b) LCST-induced supramolecular gelation: gelation of MF is only realized when the gelation temperature is above the critical transition temperature ( $T_{cloud}$ ) of LCST behavior.

132x221mm (300 x 300 DPI)

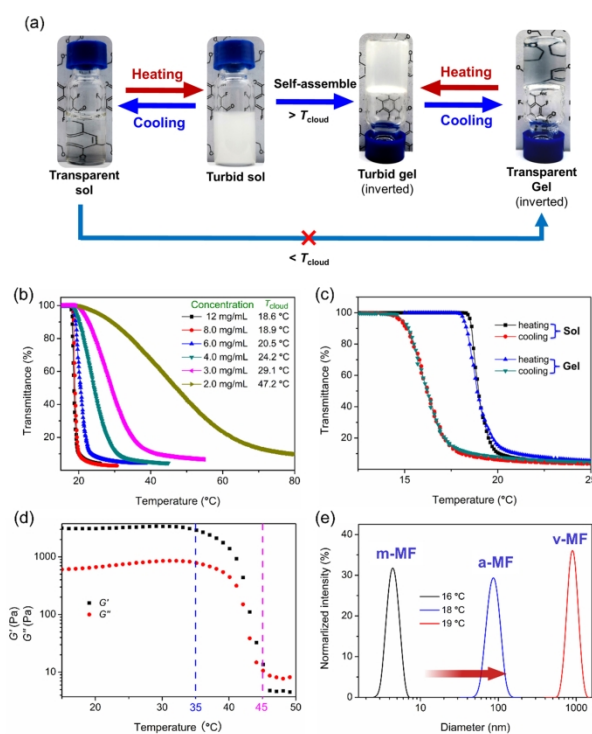


Figure 1. LCST and gelation behavior of MF: (a) macroscopic LCST-induced gelation of MF sol and gel; (b) concentration-dependent turbidity curves of MF with heating rate of 1.0 °C/min; (c) heating-cooling cycles of MF (8.0 mg/mL) at sol and gel states, with heating/cooling rate of 1.0 °C/min; (d) temperature-dependent rheology tests of MF gel (8.0 mg/mL); (e) temperature-dependent DLS of MF at a concentration of 8.0 mg/mL. Here m-MF, a-MF, and v-MF represent the monomer-type MF, aggregated MF, and visible MF, respectively.

253x190mm (300 x 300 DPI)

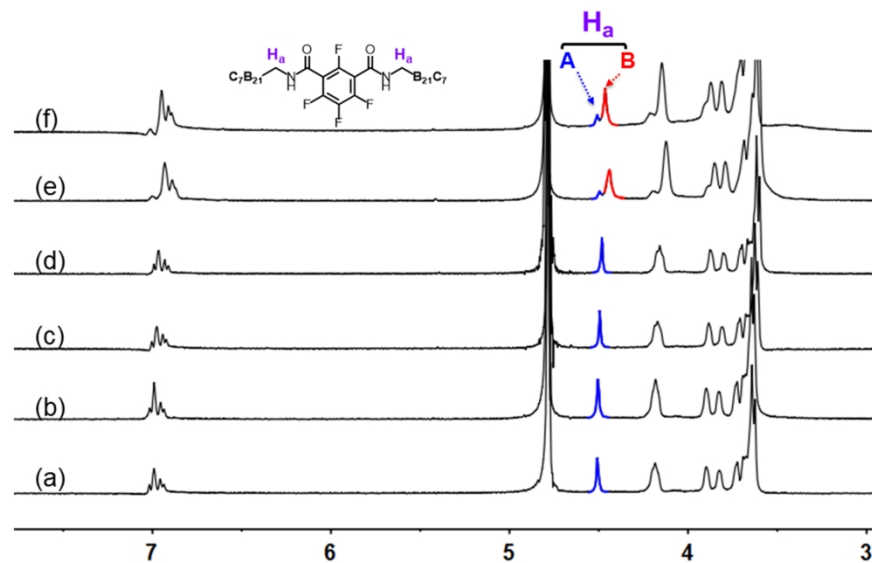


Figure 2. Concentration-dependent  $^1\text{H}$  NMR spectra ( $\text{D}_2\text{O}$ , 400 MHz, 25  $^\circ\text{C}$ ) of MF: (a) 1.4 mg/mL, (b) 3.0 mg/mL, (c) 4.0 mg/mL, (d) 5.0 mg/mL, (e) 6.0 mg/mL, and (f) 8.0 mg/mL. Here peaks A and B are in blue and red, respectively.

253x190mm (300 x 300 DPI)

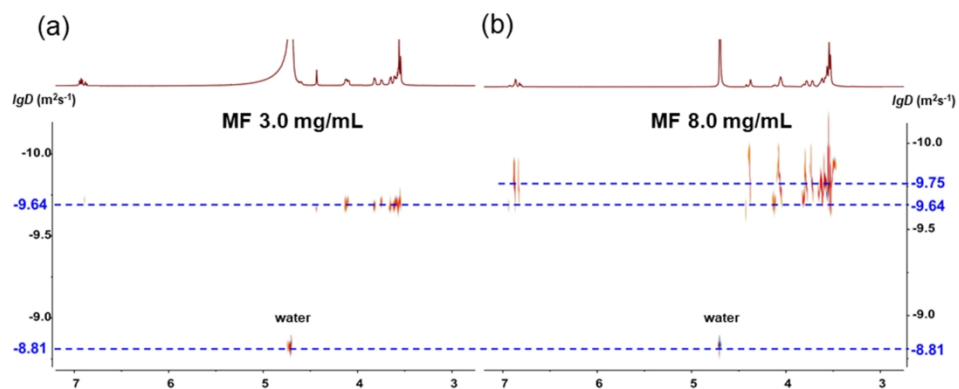


Figure 3. DOSY spectra (D<sub>2</sub>O, 400 MHz, 25 °C) of MF: (a) 3.0 mg/mL, (b) 8.0 mg/mL. The same diffusion coefficients are obtained for residual water molecules.

253x190mm (300 x 300 DPI)

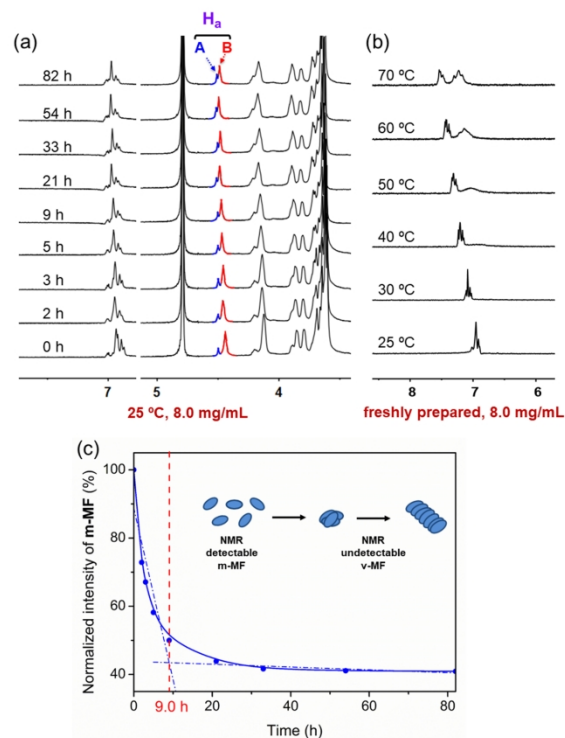
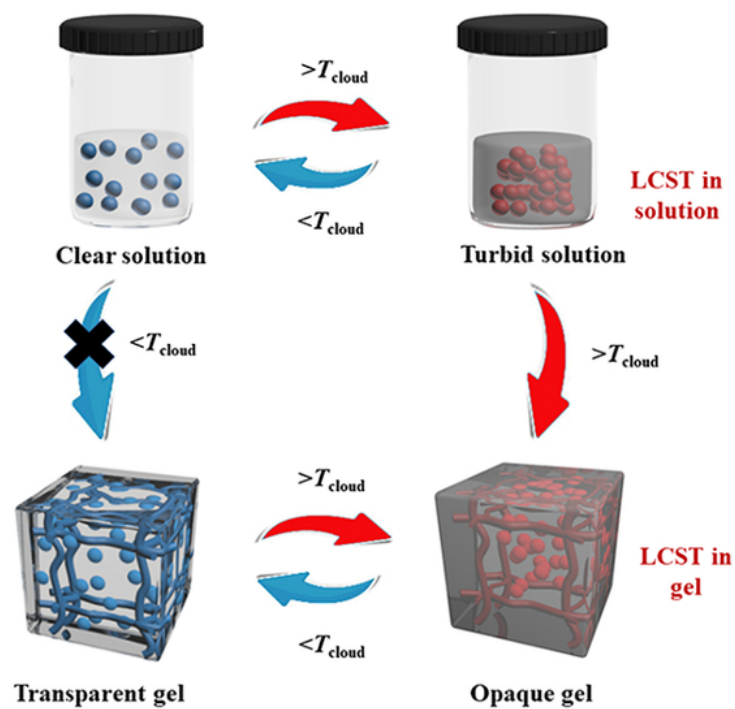


Figure 4. (a) Partial time-dependent  $^1\text{H}$  NMR spectra ( $\text{D}_2\text{O}$ , 400 MHz, 25 °C) of MF; (b) Partial temperature-dependent  $^1\text{H}$  NMR spectra ( $\text{D}_2\text{O}$ , 400 MHz) of MF. The concentrations of MF for (a) and (b) are 8.0 mg/mL. Here peaks A and B (m-MF) are in blue and red, respectively. (c) Normalized intensity of m-MF (peaks A and B in Figure 4a).

253x190mm (300 x 300 DPI)



TOC

65x46mm (300 x 300 DPI)